Mechanisms of Ionospheric Mass Escape

T. E. Moore, G. V. Khazanov, NASA Goddard Space Flight Center, Heliophysics Science Div. and Geospace Physics Laboratory

23 Aug. 2010: revision 3 for J. Geophys. Res.

Abstract

The dependence of ionospheric O^+ escape flux on electromagnetic energy flux and electron precipitation into the ionosphere is derived for a hypothetical ambipolar pick-up process, powered the relative motion of plasmas and neutral upper atmosphere, and by electron precipitation, at heights where the ions are magnetized but influenced by photo-ionization, collisions with gas atoms, ambipolar and centrifugal acceleration. Ion pick-up by the convection electric field produces "ring-beam" or toroidal velocity distributions, as inferred from direct plasma measurements, from observations of the associated waves, and from the spectra of incoherent radar echoes. Ring-beams are unstable to plasma wave growth, resulting in rapid relaxation via transverse velocity diffusion, into transversely accelerated ion populations. Ion escape is substantially facilitated by the ambipolar potential, but is only weakly affected by centrifugal acceleration. If, as cited simulations suggest, ion ring beams relax into non-thermal velocity distributions with characteristic speed equal to the local ion-neutral flow speed, a generalized "Jeans escape" calculation shows that the escape flux of ionospheric O^+ increases with Poynting flux and with precipitating electron density in rough agreement with observations.

Problem

Heating and ablation of ionospheric plasma by solar wind energy is an important atmospheric loss process that shapes Earth's magnetosphere during space storms, adding substantial plasma pressure to the magnetosphere [Moore and Horwitz, 2007]. The rate of removal of the atmosphere is non-threatening over human time scales, but is representative of a widely applicable space plasma process that played a role in removing much of the atmosphere of Mars. One possible agent of such heating and acceleration is plasma waves driven by magnetic field-aligned electric currents that transmit stresses to the auroral ionosphere. The heating should then be maximal in the auroral current sheets at about 1 R_E altitude. High altitude heating is effective in raising the flow speed of ion outflows. However, the escaping mass flux is determined by energy inputs at lower altitudes [Leer and Holzer, 1980; Moore and Horwitz, 2007] in the topside F region ionosphere, about 250-1000 km altitude.

Strangeway et al. [2005] and Zheng et al. [2005] found that two local magnetospheric factors are well correlated empirically with outflow flux: i) the precipitating magnetospheric electron density and ii) the DC electromagnetic (or Poynting) flux into the F region ionosphere. Plasma outflow resulting from soft electron precipitation can be understood [Caton et al. 1996] as the effect of ambipolar coupling of ions

and electrons. Heavy ion plasmas are also driven out of the ionosphere by wave energy dissipation and pressure acquired from the heating [Zeng and Horwitz, 2007]. The source or sources of effective waves has remained elusive, but the Strangeway and Zheng results cited above strongly suggest that the waves may be driven by ionospheric convective motions through the neutrals, since that is the principal consequence of DC Poynting flux into the ionosphere.

The requirements for ion escape flows are demanding and have been widely thought to preclude significant escape of heavy ions owing to Joule or frictional energy dissipation. The gravitational escape velocity of O^+ being approximately 11 km/s in the F region, bulk escape of ionospheric O^+ is thought to require the average O^+ ion to be given over 10 electron volts, implying a temperature of ~100,000 K. Loranc and St.-Maurice [1993] studied transient frictional heating as a method of producing ion up-flows, and they showed that transient effects produce non-thermal velocity distributions that are not well described in fluid approaches. However, they did not concern themselves with processes that turn up-flows into outflows by accelerating ions to escape velocity.

Ions are significantly accelerated transverse to the local magnetic field, suggesting that a wave generation and dissipation mechanism must operate to raise the gyration velocities of ionospheric ions. Ionospheric convective motions driven by the ac-

tive magnetosphere are typically in the range of 1-3 km/s in active auroral situations. This falls substantially short of the nominal gravitational escape velocity, 11.2 km/s, but significantly raises ion scale heights. To get outflows, modern ionospheric simulations [e.g. Barakat et al. 2003, 2006] usually invoke a combination of electron precipitation or heat flow, with application of empirically determined energy inputs often characterized as "wave particle interactions", for example by Zeng and Horwitz [2007]. The problem addressed here is the energy source and production process of the waves and acceleration required to produce observed outflow fluxes.

Strangeway et al. [2005] and coworkers cited therein also identified Alfvén waves, generated in the magnetosphere and dissipated in the ionosphere, as agents of plasma outflow, and showed that outflow flux is well correlated with the Poynting flux of AC or wave energy propagating into the ionosphere along magnetic flux tubes. Such waves may exist in the ion resonant frequency range, or may non-resonantly power outflows via the ponderomotive effect [Khazanov et al. 1998; Guglielmi and Lundin, 2001]. As important as these effects may well be, they remain problematic to derive from global magnetospheric simulations, owing to the inherent time resolution or other limitations of such models. In the future, we can anticipate a capability to specify magnetospheric wave spectra based on such models that will expand from DC to higher frequencies, and will support making such a connec-

tion with ionospheric dissipation and outflow. For the present, however, we limit ourselves in this paper to DC effects that can be extracted from current global simulations of the magnetosphere-ionosphere system.

Inasmuch as simple escape velocity arguments have been invoked to argue against important outflow effects of ionospheric convection and frictional heating, we adopt the same approach, to see if such arguments can be rebutted via a hypothesis based on ion pick-up by the convection electric field. That is, we use a generalized "Jeans' escape" calculation for ions in which the gravitational potential is reduced by the ambipolar potential and by a centrifugal potential, while the non-thermal ion velocity distribution of pick-up ions (PUI) is assessed and used to compute the fraction of the ions that are freed from gravity as reduced by this combination of effects. Subsequent sections deal with the ambipolar and centrifugal potentials, the convective pick-up process, convective transfer of energy, pick-up ion ring beam relaxation, generalized Jeans escape, and the calculation of O^+ escape flux. A discussion section is followed by conclusions.

Ambipolar Potential

The ambipolar electric field couples the energy of electrons, which would otherwise readily escape gravity, to the heavy and slow ions. The ambipolar potential simulta-

neously traps the electrons and reduces the gravitational binding of ions, allowing a fraction of them to escape. In steady state, charge balance adjusts the total ambipolar potential drop such that the net escape fluxes of electrons and ions to the magnetosphere are equal. When a superthermal population of electrons has energies substantially larger than the ion gravitational binding energy, their fractional density is effective in controlling ion escape, as is ion heating. Khazanov et al., [1997] considered the dependence of the ambipolar field and its integrated potential on the presence of un-thermalized photoelectrons. They found that the photoelectron source produces fractional densities of superthermal electrons in the range of 0.02 to 0.04 %, corresponding to a total ambipolar potential above 500 km of ~ 4-5 V, and this is consistent with observed polar wind H+ escape with relatively little O^+ escape [Abe, et al., 1993]. The photoelectrons were assumed to have a characteristic energy of 20 eV, but the results were only weakly influenced if the mean photoelectron energy was increased to 40 or 60 eV. As the fractional density of photoelectrons was varied from 0.01% to 1%, the ambipolar potential varied from about 2.9 V to 7.3 V, the variation appearing as a transition between asymptotes, as shown in Figure 1. The lower asymptote corresponds to the ambipolar potential for ion escape to match thermal electron escape. The upper asymptote corresponds to the ambipolar potential required to free enough O^+ ions to match the escape of the superthermal elec-

trons. Because the superthermal electrons are assumed to have characteristic energy significantly larger than the O+ gravitational escape energy, the required ambipolar potential is insensitive to superthermal electron characteristic energy. Because ambient O^+ ions have thermal energy substantially less than their gravitational escape energy, the required ambipolar potential saturates as it approaches bulk thermal O^+ escape, which increases steeply with incremental further increase in ambipolar potential. Enhanced heavy ion escape owing to other factors such as ion heating or acceleration effects will similarly limit or suppress the ambipolar potential to a value less than that otherwise needed to balance ion and superthermal electron escape.

Secondary electrons are produced by primary electrons of magnetospheric origin and have the same interaction with ionospheric outflows as photoelectrons, via the ambipolar potential. The shape of the low energy secondary electron distribution also steepens toward the low thermal energies because of collisional plasma thermalization processes, but may differ in detail from the photoelectron spectrum. Nevertheless, because their characteristic energy is greater than the O^+ binding energy, the ambipolar potential is insensitive to the spectrum details and is driven by the superthermal electron partial density, as shown in Figure 1.

For present purposes, we assume that the precipitating electron density identified by Strangeway et al. [2005] characterizes the auroral secondary electron population and is proportional to the fractional superthermal electron density of Khazanov et al., [1997], with the constant of proportionality regarded as a free parameter to be determined. Electron precipitation was evaluated for E > 50 eV in the former study, while the latter study considered the entire superthermal electron distribution, taken to have a characteristic energy of 20-60 eV. Since the density of electrons > 50 eV is necessarily much less than the full density of superthermal electrons without such a lower limit, the total density of electrons that produces the correct ratio N_p/N_{tot} will be smaller than typical local electron densities by a factor that depends upon the actual shape of the superthermal electron velocity distribution. Figure 1 displays a hyperbolic tangent fit to the relationship found by Khazanov et al., [1997], together with the fitting parameters and their fitting uncertainties. This ambipolar potential reduces the gravitational escape velocity for ionospheric ions, as a function of precipitating electron density, according to the relationship:

$$v_{esa} = \sqrt{\left(\frac{2GM_E}{(H_{exo} + R_E)} - \frac{2q\Phi_{AP}}{M_i} \right)} \qquad (1)$$

where G is the gravitation constant, M_E and R_E are the mass and radius of Earth, H_{exo} is the exobase height, q is the elementary charge, and M_i is the ion mass. The present

work would clearly benefit from more comprehensive precipitating electron observations without a lower energy limit. This is an important target for future observational research in this area, because a plentiful supply of superthermal secondary electrons will cause the ambipolar potential to rise to the level where thermal ion escape is incipient and requires only a small amount of additional energy to become a large bulk escape.

Centrifugal Acceleration

A prominent source of energy for ion acceleration is convection driven by magnetic coupling with magnetospheric hot plasma motions. Terrestrial F-region convection is much slower than solar wind or magnetospheric flow speeds, owing to the large ratio of magnetic field intensities. However, ionospheric convection is comparable to or exceeds neutral gas thermal speeds. It also increases steeply with altitude, such that higher altitude plasmas on the same flux tubes may approach the gravitational escape speed, independent of ambipolar effects. These parameters are illustrated in Figure 2. Here the Poynting Flux at 4000 km altitude has been set to 1, 10, and 100 mW/m^2 so the system is driven across the effective range observed in the Strangeway [2005] study, for a typical value (8 S) of dayside auroral ionospheric [Strangeway, private communication].

The increase in the convection speed with altitude shown in Figure 2 gives rise to a centrifugal acceleration effect [Horwitz et al., 1994; Demars et al., 1996]. Plasma ions flowing along rapidly convecting magnetospheric flux tubes are accelerated as both perpendicular and parallel energy are acquired from the convection electric field. Ions gain equal amounts of perpendicular and parallel energy, equal to the convection speed at any altitude, adjusted for gravitational accelerations parallel to the magnetic field [Horwitz et al., 1994]. Centrifugal forcing depends weakly on convection path and field curvature details, but for convection across the pole of a dipole field (their equation 4b), at altitudes lower than a few R_E it is approximately:

$$F = 1.5 m V_{conv}^2 \frac{r^2}{R_E^3} \qquad (2)$$

This centrifugal force can be expressed as the gradient of a potential:

$$\Phi = \frac{1}{2} m v_{conv}^2 \left(\frac{r}{R_E} \right)^3 \qquad (3)$$

This reduces the escape speed everywhere via the subtraction of an additional term from equation (1), yielding equation (4).

$$v_{esa} = \sqrt{\frac{2GM_E}{(H_{exo} + R_E)} - \frac{2q\Phi_{AP}}{M_i} - v_{conv}^2 \left(\frac{r}{R_E} \right)^3} \qquad (4)$$

The escape speed falls to zero at the levels shown in Figure 2, for different values of the Poynting flux (or convection speed), with zero ambipolar potential. Non-zero values of ambipolar potential clearly reduce the escape speed further. Above the convection (and ambipolar) dependent altitude where escape speed drops to zero, which we term the "centrifugal horizon," even cold ions continue to move upward and are accelerated further. This height is lowered by strong convection. However, in the topside ionosphere, below the exobase, the escape speed is not reduced by a substantial amount, and additional acceleration is needed to overcome gravitational binding, even when convection is very strong. Thus, as shown by Demars et al., [1996], centrifugal acceleration alone is not a significant effect on outflow *flux*, thought it is important in accelerating the outflows, with obvious effects on their circulation in the magnetosphere. It is included here mainly for completeness.

Convective Pick-up

The generation of ion-resonant diffusive waves is familiar from other situations where photo-ionization creates new ions with initial velocities of the parent cold neutral atoms, which are then "picked up" by the local plasma motional electric field. Pick-up is distinct from dissipation of horizontal currents in the lower parts of the ionosphere where ions are collision dominated, usually known as Joule or frictional

heating. The pick-up process operates at altitudes where collisions with atoms or molecules are rare compared with gyrations, and photo-ionization or charge exchange dominate ion-neutral interaction, that is, above ~125 km altitude [Kelley and Heelis, 1989], a boundary to which we refer as the "isotropause." Above that level, magnetic anisotropies can be created and persist without being isotropized by collisions. Most of the F-layer is above the isotropause, including its "topside" extending to the exobase, defined as the altitude where the mean free path exceeds the scale height of the scattering neutral gas. The exobase lies in the range from 500 to 1300 km altitude [Banks and Kockarts, 1973], increasing linearly with the neutral thermospheric temperature during periods of active Joule heating.

Pick-up ion (PUI) distributions are produced by convection of ions through the neutral gas, when ions are created in the neutral gas frame by photo-ionization (if sunlit) or by charge exchange between ions and neutrals, or to a lesser extent by scattering collisions of the drifting ions with stationary neutrals. Examples include the interstellar gas flow throughout the solar system [Bogdan et al., 1991], or the localized gas sources at un-magnetized planets, satellites, and comets [Szegö et al., 2000]. PUI are the accelerated cold ions, after a gyro-period, during which they are picked up by the convection electric field as seen in the neutral frame, gaining drift and gyration speed each equal to the convection speed [Kivelson & Russell, 1995, p.206].

The result is a ring or toroidal velocity distribution, or a "ring beam", rooted in the neutral frame and encircling the convecting plasma frame with a diameter of twice the plasma convection speed in velocity space. This mechanism was studied in an ionospheric context during the 1970's, reviewed by St-Maurice and Schunk, [1979], revisited by Barakat et al., [1983], Winkler et al. [1992], Wilson [1994], Barghouthi et al., [1994], and Hubert and Leblanc [1997]. PUI are an inevitable consequence of moving driver plasma that is magnetically linked to a partially ionized "anchor" gas, in the altitude range where collisions are important but infrequent relative to the local gyro frequency.

The geomagnetic field couples magnetospheric convection into the ionosphere as shown in Figure 2, but the plasma motion is opposed by drag owing to ion collisions with the gas atoms, which also demagnetizes the ions and allows transverse current to flow in the low F region, principally below the isotropause. Maxwell stresses (**JxB**) drive ionospheric plasma flow and retard the conjugate magnetospheric flow, transmitted by field-aligned electric currents. The ionospheric flow is powered by the Poynting energy flux from the driver plasma into the convecting ionospheric plasma. Thus, either Poynting flux (F_P) or plasma flow can be regarded as the driver, but we adopt F_P as the driver to facilitate comparison with the results of Strangeway [2005]. Given fixed Fp, ionospheric convection speed depends on the ionospheric

conductance. But in either case, the ionospheric height integrated conductance (Σ_P) is the load on the electric circuit or on the driving motions, and the convection speed corresponding to a particular value of F_P flowing into the ionosphere is given by:

$$v_{conv} = \frac{1}{|B|}\sqrt{F_P/\Sigma_P} \qquad (5)$$

Conductance distributions given by Ridley et al. [2004] are representative, indicating a range of $\sum_P$ from 2-20 Siemens, representative of the entire dayside region and polar cap under a wide range of conditions, and compatible with 8 S as a typical value. For given Poynting flux, convection speeds will be correspondingly lower in the low latitude dayside or night time auroral zone, but Poynting flux may also be larger, with compensating effect on the magnitude of ionospheric convection speed.

Ring Beam Relaxation

In practice, ring beams have proven difficult to observe, consistent with rapid relaxation into non-thermal but transversely accelerated distributions. Ion species self-collisions are expected to erode and thermalize ring beams [Barghouthi et al., 1994] on collisional time scales. On faster plasma time scales, unstable velocity distributions will be eroded away by plasma waves. Any velocity distribution with positive $\partial f(\mathbf{v})/\partial v$ has free energy available to drive wave growth that removes the

free energy feature by diffusing particles from higher to lower phase space densities and predominantly, though not exclusively, from higher to lower energy. The diffusion occurs along characteristics specific to the driven wave modes. The magnitude of $\partial f(\mathbf{v})/\partial v$ and corresponding wave growth driven by the ionospheric PUI feature are compounded in the topside ionosphere by the highest phase space densities and lowest characteristic speeds anywhere in the space environment. As a result, one expects to observe distributions that are marginally stable with $\partial f(\mathbf{v})/\partial v \leq 0$. St.-Maurice and Schunk [1979] cited plasma observations of the ring feature without a pronounced minimum at zero velocity. The ratio of the ring speed to neutral thermal speed (often referred to as D*) never exceeded 1.5 in that study, even when ion temperature suggested a D* of 2 to 3 or more. Space and time variability of the ionosphere is also a significant problem for observations, making it difficult to capture a ring beam feature [Moore et al., 1996]. High altitude long-lived observations indicating a core ring beam features have been reported [Moore et al., 1986], but are rare. The above facts are consistent with ring beam production of intense waves that quickly erase the velocity space instability responsible for them.

In contrast, many observations have been made of "transversely accelerated ions" or TAI, and their close relatives, ion conics [Moore and Horwitz, 2007]. Conics develop as transversely accelerated ions move upward while slower ions remain relatively

stationary. The prevalence of auroral TAI and ion conics requires that transverse energy diffusion be faster than pitch angle diffusion in the auroral context. Figure 3 shows observations by the Swedish Freja spacecraft [André et al., 1994]. The perpendicular velocity distribution is a power law that could be approximated as exponential for low speeds. The thermal core of this distribution, if any, is at velocities lower than the range observed. At higher speeds, the distribution is well fit by a generalized Lorentzian or power law with $(v/v_{scl})^{2.2}$ as argument, as indicated in Figure 3 and identified in Table 1. André et al. [1994] simulated the effect of the observed ambient wave populations at Freja and concluded that the observed waves would heat ions so as to produce the observed hot tail distributions. The open question is that of the source of the waves that heat the ions, principally in the transverse direction. Local wave growth owing to a ring beam feature was derived by Post and Rosenbluth [1966], but in the context of the loss cone instability. Such waves are commonly observed in the topside ionosphere under conditions of strong convection [St-Maurice and Schunk, 1979]. Significantly, a number of reports of incoherent scatter radar echo spectra have been interpreted as the result of backscatter from plasmas with a toroidal or ring beam velocity distribution [Suvanto et al., 1989; Kinzelin and Hubert., 1988].

Bogdan et al., [1991] interpreted shell distributions in interplanetary space as products of the PUI process. Near comets, plasma analyzers encounter PUI populations [Neugebauer et al., 1990], and deeper in the coma, "thermalized" exponential or power law tails attributable to them [Mukai, 1986; Richardson et al. 1987]. Theoretical work has treated the instability in the high velocity outer coma [Lee and Gary, 1991], and as a function of distance extending deep into the inner, collisional coma [Puhl et al,. 1993], using a velocity diffusion equation with empirically determined coefficient in the latter case. However, the general self-consistent quasi-linear evolution problem has not evidently been solved.

Quasi-linear plasma theory describes diffusion along characteristics that are circles centered on ± V_A (Alfvén speed) in the weak-field, high-speed, collisionless regime. Velocity diffusion along such circles centered near the origin in velocity space, relative to the ion ring beam, takes the form of pitch angle diffusion and forms bispherical shell distributions [Szegö et al., 2000], with little energy diffusion. Deeper in a cometary coma, ion flow velocities fall to much smaller than V_A. Then, as for the Earth's ionosphere, diffusion characteristics are circles centered at large parallel velocities, which cut transversely through the ring beam. Also, dispersive ion cyclotron waves may become important, with non-circular diffusion characteristics [Isenberg

and Vasquez, 2007]. In either case, velocity diffusion of the PUI feature is transverse to the magnetic field, and pitch angle diffusion is relatively weak.

Puhl et al. [1993] simulated coma PUI ring beam "thermalization" and found a power law form that could also be approximated as exponential at low speeds. They found the "temperature" of the relaxed distribution to correspond to a thermal speed equal to double the local convection speed (their figure 6b), or the bulk plus gyration velocity of ions in the frame of the neutrals. However, this "temperature" was derived as a moment of highly non-thermal power law velocity distributions. We take the scale velocity for all distribution forms to be equal to the local convection speed, representing the gyration energy in the convecting ion frame of reference. The bulk convection speed is also used to evaluate the centrifugal potential.

The above simulation results were supported by a relevant active experiment reported by Paterson and Frank [1989] and Gurnett et al. [1988]. They observed a power law tail of hot ions in the wake of the space shuttle, from the Plasma Diagnostic Package, and inferred that charge exchange between shuttle out-gassing and ionospheric ions produced new ions in the shuttle frame, which were then "picked up" into the ionospheric plasma frame, producing ring beams that generated the observed waves and subsequently turned into hot transverse ion distributions with measurable fluxes up to 100 eV. We find that the observed distributions are well fit

by a kappa distribution with kappa ~ 2.75 and a characteristic speed of ~ 3 km/s. These ion distributions remained transversely peaked and did not form spherical shells as is the case for cometary ion pick-up, consistent with the high Alfvén speed in the ionosphere and diffusion principally transverse to the local magnetic field.

From the above, we conclude that ion ring beam distributions relax through perpendicular velocity diffusion, in the low speed, high-V_A context appropriate to the ionosphere or inner coma of comets, both in theory and in practice. An extended transverse velocity distribution is expected to form, having power law dependence at higher speeds, with scale speed equal to the local convection speed. Incidentally, we note the ubiquitous presence of power law tails in space plasmas, which may be understandable if ion pick-up is similarly ubiquitous. In any case, we adopt this simulated and observed distribution to assess ion escape. We note that any other source of waves that produces power law tails scaled with the local convection speed would be equally effective in producing the results given below.

Important assumptions of this approach should be noted: First, unstable waves are assumed effective in relaxing the distribution as soon as the ion convection speed becomes an appreciable fraction (10-30%) of the neutral thermal speed. This is the same condition required for a perceptible local minimum to form in the velocity distribution owing to the gyration of newborn ions and thus seems justifiable. How-

ever, a full ring beam instability analysis must be done to substantiate this assumption. Second, it is assumed that the generated wave intensities, like other imposed wave intensities discussed above, have an insignificant ponderomotive effect on the ions [Khazanov et al., 1998]. Such a ponderomotive effect would enhance outflow above the values obtained here, so this is a conservative assumption that nevertheless may cause the present results to underestimate outflow fluxes. Finally, we assume that the time scale for such power law distributions to relax to Maxwellian would be a collisional time scale much longer than the wave particle diffusion time scales responsible for creating the power laws.

Generalized Jeans' Escape

The standard assessment of O^+ escape is that such escape requires on the order of 10 eV to be imparted to each escaping ion, so that it can overcome Earth's gravitational binding. Equivalently, this requires each O^+ ion to be accelerated to 11.18 km/s, the "escape velocity" for Earth. The typical temperature of oxygen in the ionosphere being of order 3000 K, or about 0.03 eV, corresponding to a thermal speed of only about 300 m/s, typical oxygen ions must gain most of 11 km/s to escape. This argument is a direct application of Sir James Jeans [1904] approximate method for calculating the rate of loss of gas atoms from a planet. At the exobase, above which

the mean free path exceeds the scale height so that upward motion is free of collisions, the species density and thermal velocity, (that is, the species thermal or limiting flux) are multiplied by a factor corresponding to the fraction of the atoms with velocities exceeding the escape velocity. This simple method has been shown to exaggerate the H and He escape rates by about 3-30% [Brinkman, 1970], but this level of accuracy is more than sufficient for present purposes.

We generalize the Jeans method, adapting it for ion escape in two ways. First, we consider non-thermal forms of velocity distribution in addition to thermal Maxwellians [see also Shizgal and Arkos, 1996]. Table 1 provides a listing of the forms used. Second, but just as important, we consider additional potentials that act on ions, namely the ambipolar electric field and centrifugal force, as discussed above. We estimate the escape flux as the product of the limiting flux for O^+ at the exobase and a factor corresponding to the fraction of the ions exceeding the exobase escape velocity. We treat velocity in one dimension, because perpendicular velocities become parallel velocities (in the source cone) for free ion motion above the exobase, conserving the first invariant.

Oxygen Escape Flux

We next use the "generalized Jeans escape" estimate described above to evaluate the dependence of ion escape on Poynting flux and electron precipitation, evaluating escape at the exobase. Also relevant is the O-H density crossover, above which fast O^+ charge exchange produces mainly cold H+ ions, rather than cold O^+ ions. This occurs near the exobase, with a similar dependence on thermospheric temperature [Moore, 1980]. Scattering collisions with neutrals continue to be important above this altitude, with the effect of maintaining and enhancing the PUI feature, as convection speed increases. Scattering collisions with neutrals interrupt ion drift motions and randomize them about the neutral gas frame, such that they are again picked up by the electric field, albeit with less contrast between their gyrating drift motion and their random motions than for charge exchange. Scattering collisions with other ions, on the other hand, tend to relax the ring beams into transversely heated velocity distributions. We neglect these competing effects and indeed all such processes above an exobase taken at 500 km, regardless of Poynting flux. This conservative approach ignores the rise in the exobase height with thermospheric temperature, even as most of the Poynting flux goes into frictional heating of the neutral gas. It will therefore tend to produce underestimates of the escape flux dur-

ing very disturbed conditions that raise the effective exobase as the thermosphere heats up.

The escape flux of O^+ is limited by photo-ionization sources and friction with thermospheric gas. The limiting flux has been computed via a full ionospheric topside simulation [e.g., Barakat et al., 1987]. It depends on many factors including solar activity, F-peak density, influenced both by photo-ionization and horizontal transport, and the topside scale height of the neutral gas, influenced by Joule heating. Both photo-ionization and charge exchange contribute to the production of ions from cold neutrals. Active solar conditions produce nearly 10^3 O^+ $cm^{-3}s^{-1}$ at 125 km altitude [Banks and Kockarts, 1973, p.B-114]. Integration over a scale height of 100 km above that supports a flux of 1 x 10^{10} $cm^{-2}s^{-1}$. A similar cold ion creation rate applies to O^+-O charge exchange [Banks and Kockarts, 1973, p.A-224], if we take $n_{O+} \sim 10^5$ cm^{-3}, and $n_O \sim 10^7$ cm^{-3} [Kelley and Heelis, 1989, p.6] with 100 km scale height. We thus have an adequate source of cold ions for pick-up to provide an O^+ limiting flux (at 4000 km altitude) of ~ 2 x 10^{10} $cm^{-2}s^{-1}$, which is the largest flux observed by the Polar TIDE investigation [unpublished white paper]. This is also the lowest value consistent with the lack of apparent saturation evident in the Strangeway et al. [2005] results, shown as the background of Figures 4-6. Higher production would follow from the enhanced supra-auroral O densities derived from recent spacecraft

accelerometer results showing storm enhancements of oxygen density above auroral features by a factor of 3 to 8 [Bruinsma et al., 2006]. Despite the constraints cited above, it must be appreciated that this value is a parameter of the simple model used here.

The available Poynting flux, evaluated at 4000 km, in conjunction with the ionospheric conductance, determines the convection speed profile of the flux tube, which is then evaluated at the exobase. There, we assume the ring beam relaxes into a transverse power law, scaled by the local convection speed, as simulated and observed by Freja, in the form predicted by the Puhl et al., [1993] simulations. The fraction of the distribution that extends above the local escape speed, evaluated at the exobase, is taken to be the fraction of the local density that will escape. Thus, the partial density of the distribution that exceeds the escape speed (for the exponential velocity distribution, as an example) is:

$$n_{partial} = \frac{n}{v_{th}} \int_{vesc}^{\infty} \exp\left(-\frac{v}{v_{th}}\right) = n \exp\left(-\frac{v_{esc}}{v_{conv}}\right) \qquad (6)$$

For a Lorentzian, the corresponding cumulative function is an arctangent, while for a Maxwellian, it is the complementary error function, erfc. These are used to compute the escaping fraction of the distribution, as summarized in Table 1.

The escape flux is estimated as the hemispheric flux, assuming that transverse energy becomes parallel energy owing to magnetic flux tube divergence, and so is obtained as the product of the fractional density with the scale speed, taken to be v_{conv}: again for an exponential distribution, where $F_{lim} = nv_{conv}$.

$$F_{esc} = n_{partial} v_{conv} = F_{\lim} \exp\left(-\frac{v_{esc}}{v_{conv}}\right) \qquad (7)$$

The results of this integration of the escape flux are shown in Figure 4 for ionospheric conductance of 8 S, in three cases, each with three sub-cases:

First, we considered the result for escape of a generalized Lorentzian (power law) velocity distribution with scale speed equal to the convection speed at the exobase and with exponent matching the fit to the Freja data of André et al., [1994]. The downward shifted curve of similar shape indicates the result if the ambipolar potential is ignored, while the nearly coincident dashed line indicates the same result if the centrifugal potential is ignored.

Second, we considered an exponential velocity distribution with scale speed given by the convection speed at the exobase. Again, the downward shifted curve indicates the result if the ambipolar potential is ignored, while the nearby dashed curve indicates the result if the centrifugal potential is ignored.

Finally, we considered a ring beam that has relaxed fully to a Maxwellian with thermal speed given by the convection speed at the exobase, again with a parallel curves showing the results when ambipolar and then centrifugal potential is ignored. A plot of the Strangeway et al. [2005] data set and fit serves as background of Figure 4.

The value of Poynting flux corresponding to D* = 0.3 is indicated on the plot to suggest a level at which the ring beam feature is appreciable, but as far as we know, no one has determined the threshold value of this parameter for wave growth.

In Figure 5, we display the same results, in the case of the Lorentzian distribution, including centrifugal potential, for several different values of N_p and corresponding ambipolar potentials. Insofar as the ambipolar potential is independent of the Poynting flux, the variations with N_p explain some of the observed scatter in the escape flux data. A bold dashed curve cuts across the other traces as Poynting flux increases, obtained by requiring the precipitating electron density N_P to track the Poynting flux according to the Strangeway et al., [2005] fits to the observations. This implements the reported fact that the two quantities are correlated, presumably resulting from common magnetospheric processes, with larger Poynting flux accompanied by larger precipitating electron densities. Again, the value of Poynting flux corresponding to D* = 0.3 is indicated on the plot to show where the velocity distribution becomes perceptibly toroidal.

Figure 6 displays a plot of the dependence of escape flux on precipitating electron density, N_P, for various assumed constant values of Poynting Flux. As in Figure 5, a bold dashed trace again represents the result of tying N_P to F_P according to the Strangeway et al. [2005] fits. Clearly, independent behavior of these two parameters is capable of producing scatter in the results. Evidently, though the electron precipitation and ambipolar potential are both significant effects, they are not as powerful as the Poynting Flux in reproducing the observed large dynamic range of outflow flux.

To summarize, little or no escape would be expected, at any but the extreme highest Poynting flux levels observed, after the distribution relaxes to a Maxwellian thermal speed corresponding to the local convective pick-up speed. Escape is appreciable at lower power levels if the velocity distribution at the exobase is an exponential with the local convection speed as scale speed. The escape response best mimics the observed (eyeball fit) empirical behavior for the Lorentzian power law distribution. When electron precipitation alone is assumed to drive the ambipolar potential, the result is a modest increase of escape flux at any Poynting flux level, an effect that nevertheless appears strong when coupled with a correlated Poynting Flux variation.

Discussion

Figure 7 is a schematic flow chart of the mechanisms described above, based loosely on the flow chart of Strangeway et al. [2005], but with the addition of an evaluation of the effects of ambipolar potential, centrifugal forcing and convective ion pick-up, and an allusion to neutral gas upwelling effects. The ambipolar electric field extends far above the exobase and is lumped into a total potential above the exobase. Centrifugal forcing also extends far above the exobase, lowering the height at which gravitational escape occurs. But while it may have strong effects on outflow speeds, we found that it only slightly reduces the escape speed for ionospheric ions at the exobase. The main effect of neutral gas upwelling is to raise the exobase, but we have not computed that effect here.

Figure 7 also indicates the hypothetically important role of ion pick-up by convection in producing unstable velocity distributions that drive waves to relax the ions into transversely accelerated power law distributions. The observed and modeled transverse velocity distribution at the exobase, acting in conjunction with the ambipolar potential driven by precipitating electron thermal energy, implies increasing escape as ionospheric convection speed and electron precipitation increase, producing wholesale escape of much of the velocity distribution for high values of the

Poynting flux that powers such convection, and-or of the precipitating electron density that accompanies it.

The results imply that the form of the ion velocity distribution maps directly into the observed dependence of escape on DC Poynting flux. A power law distribution gives the best agreement with the Strangeway et al. [2005] (power law) results, while a less extensive exponential distribution (in v) would suppress escape at lower levels of Poynting flux. Full thermalization of PUI ring distributions to a Maxwellian form would suppress outflow to well below the observed response at all power levels, even with substantial precipitating electron density, demonstrating the need for active wave particle ion acceleration. Variations of the actual velocity distribution produced are likely to be responsible for much of the scatter present in the observations, though we have also shown that ambipolar potential variations are capable of contributing to the scatter.

The curves in Fig. 5-6 give a reasonable eyeball fit to the FAST observations, suggesting that the power law distribution predicted by the simulations of Puhl et al. [1993] are realistic, as also observed in the ionosphere by the space shuttle Plasma Diagnostic Probe and Freja, at higher altitudes. Still it is clear that a more complete understanding of low energy ring beam relaxation via wave particle interactions is critically important to the proposed mechanism of plasma escape. The Puhl et al.,

[1993] calculation is the only theoretical basis of which we are aware for ring beam relaxation into power law tails, as used here. As a semi-empirical parametric result, it is perhaps the weakest assumption in the proposed model, despite its successes. Further study of PUI ring beam relaxation is likely to yield significant results, possibly leading to a better understanding of the ubiquity of power law tails in space physics. If this paper motivates such study, it will have served its intended purpose.

Four mechanisms are often invoked to explain ionospheric mass escape: i) heating of the F-region electron gas by addition of superthermal electrons, increasing the ambipolar potential, ii) Joule or frictional ion and neutral gas heating, raising scale heights and supply of plasma without escape, iii) resonant ion transverse acceleration (or ponderomotive forcing) by particle interactions with waves of unspecified source; and iv) centrifugal acceleration reducing the escape speed at the exobase. The results presented here suggest that convection of plasma relative to neutral gas is an important source of free energy (in toroidal PUI ring beams) for waves that accelerate ions near and below the exobase. Other wave sources are also likely to be important, but toroidal PUI distributions are a distinctive feature of ionospheric convection. The latter three mechanisms all respond to the speed of convection and thus to the amount of electromagnetic power (Poynting flux) from the linked magnetospheric or solar wind plasmas. Mechanism iii) converts bulk motion into disor-

dered but non-thermal transverse ion energy that increases the number of ions that overcome gravity, as reduced by the ambipolar and centrifugal potentials. Mechanism iv) has been shown to operate at too high altitudes to be an significant contributor to escape fluxes, though it clearly accelerates outflows at higher altitudes and thus affects their ultimate destinations or escape from the magnetosphere.

These "generalized Jeans escape" results suggest a theoretical basis for the empirical relationships of Strangeway [2005], identifying a new but important source for the waves that heat ionospheric ions, directly driven by convection and hence by DC Poynting flux. But this must be fully tested in future topside transport modeling. Also, a full understanding of the proposed process requires a solution of the quasi-linear relaxation of ring beams to determine its details and time scales and to further understand and validate the form of the velocity distribution that is formed.

The hypothetical mechanism modeled here is motivated by the observed correlation of outflow with ionospheric convection as driven by DC Poynting flux. It is compatible by design with multiple features of auroral ion outflows, including their transverse heating in response to convection, response to electron precipitation, power law tails, and production of broadband ion-resonant waves. The results do not prove that there is no other source of the effective waves driven by Poynting flux, but they

do show that another source is unnecessary, given the operation of the mechanism as proposed. Two key tests of the proposed mechanism can be envisioned:

If the asserted power law tails are rare at the exobase, or if their scale velocity correlates poorly with convection and Poynting flux, a different source of waves is implied.

If another source of ion resonant wave energy is better correlated with DC Poynting flux or convection strength, it would refute this model.

It has often been observed that powerful ionospheric escape events, referred to as ionospheric mass ejections [Moore et al., 1999], often contain appreciable amounts of the molecular ions N_2^+ and NO^+. Wilson and Craven [1998] showed that such events were associated with strong and prolonged (> 15 min) convection of the ionosphere. They argued that the heating required to lift molecular ions up to high altitudes might be provided by waves driven unstable by toroidal O^+ distributions. Such events are certainly increasing molecular scale heights, leading to formation of new molecular ions in sunlight or through charge exchange with the more abundant ion species. Thus it may also be profitable to consider the formation of toroidal pick-up distributions of the molecular ions. These should be more toroidal than those of O^+, since the molecular thermal speeds are smaller by a factor of ~2 than those of O.

Thus it should be expected that enhanced molecular densities in the topside would lead directly to enhanced molecular ion upflow and outflow, assuming the mechanism suggested here is equally effective in generating power law molecular transverse velocity distributions. An assessment of molecular escape owing to ambipolar pick-up is beyond the scope of the present paper but would be a natural future outgrowth of this work.

Conclusions

A model of ionospheric ion acceleration and outflow has been hypothesized on the basis of the following assumptions based on cited publications:

i) Precipitating electrons are assumed to produce a superthermal secondary electron population for which the ambipolar potential relation of Khazanov et al., [1997] applies. The fraction of the superthermal electron density above 50 eV is treated as a free parameter.

ii) PUI ring beams form in the F region up to the exobase owing to convection of ions relative to neutrals, as described by St.-Maurice and Schunk [1979]. Ions are assumed weakly collisional but magnetized. The exobase height is an important parameter.

iii) As D* becomes appreciable (>0.1-0.3), PUI ring beams are assumed to generate broadband ion resonant waves that fill the depression at center of the ring beam, but also diffuse ions upward in energy (though always downward in phase space density), creating non-thermal power law velocity distributions with scale speed = V_{conv}.

Based on a simple "generalized Jeans escape" calculation, we find that escaping O^+ flux increases with Poynting flux (and associated convection) and with electron precipitation in rough agreement with empirical scaling relationships of Strangeway et al., [2005]. The escape limit, F_{lim}, is treated as a parameter, the emphasis here being on the functional dependence on drivers rather than the absolute limiting flux.

Acknowledgments

The NASA LWS TRT program supported this work under WBS 936723.02.01.03.82. This work was inspired by the ideas of J.-P. St-Maurice and discussions with Rickard Lundin. The authors thank Thomas Cravens, Pamela Puhl-Quinn, and Peter Gary for helpful discussions. Philip Isenberg and Martin Lee were especially helpful in understanding Alfvén wave and ion cyclotron heating. The authors thank the reviewers of this and an earlier version of this paper submitted to Geophys. Res. Lett., Mei-Ching Fok and Alex Glocer for critical readings of the manuscript.

References

Banks, P. M., and G. Kockarts (1973), Aeronomy, Academic, New York.

Abe, T., B. A. Whalen, A. W. Yau, S. Watanabe, E. Sagawa, and K. I. Oyama (1993), Altitude profile of the polar wind velocity and its relationship to ionospheric conditions, Geophys. Res. Lett., 20, p. 2825.

André, M., et al. (1994), Transverse ion energization and wave emissions observed by the Freja satellite, Geophys. Res. Lett. 21, 17, pp.1915-1918.

Barakat, A. R., R. W. Schunk, and J. P. St.-Maurice (1983), Monte carlo calculations of the O+ velocity distribution in the auroral ionsphere, J. Geophys. Res. 88(A4), 3237.

Barakat, A. R., et al., 1987, Ion escape fluxes from the terrestrial high-latitude ionosphere, J. Geophys. Res. 92, p.12255.

Barakat, A. R., and R. W. Schunk (2006), A three-dimensional model of the generalized polar wind, J. Geophys. Res., 111, A12314, doi:10.1029/2006JA011662.

Barakat, A. R., R. W. Schunk, and H. G. Demars (2003), Seasonal and solar activity dependence of the generalized polar wind with low-altitude auroral ion energization, J. Geophys. Res., 108(A11), 1405, doi:10.1029/2002JA009360.

Barghouthi, I. A., A. R. Barakat, and R. W. Schunk (1994), A Monte Carlo simulation of the effect of ion self-collisions on the ion velocity distribution in the hig-latitude F-region, Ann. Geophys., 12, 10/11, p.1076.

Bogdan, T J, M A Lee, P Schneider (1991), Coupled Quasi-Linear Wave Damping and Stochastic Acceleration of Pick-up Ions in the Solar Wind, J. Geophys. Res., VOL. 96(A1), pp. 161-178.

Brinkman, R. T. (1970), Departures from Jeans' escape rate for H and He in the Earth's atmosphere, Planet. Sp. Sci. 18, 4, p.449.

Bruinsma, S., et al. (2006), Thermosphere density response to the 20-21 November 2003 solar and geomagnetic storm from CHAMP and GRACE accelerometer data, J. Geophys. Res. 111, p. AO6303, doi. 10.1029/2005JA011284.

Caton, R., J. L. Horwitz, P. G. Richards, and C. Liu (1996), Modeling of F-region up-flows observed by EISCAT, Geophys. Res. Lett., 23, 1537 – 1540.

Cully, C. M., E. F. Donovan, A. W. Yau, and G. G. Arkos (2003), Akebono/Suprathermal Mass Spectrometer observations of low-energy ion outflow: Dependence on mag-netic activity and solar wind conditions, J. Geophys. Res., 108(A2), 1093, doi:10.1029/2001JA009200.

Demars, H. G., A. R. Barakat, and R. W. Schunk (1996), Effect of centrifugal acceleration on the polar wind, J. Geophys. Res., 101(A11), p.24,565.

Guglielmi, A., and R. Lundin (2001), Ponderomotive upward acceleration of ions by ion cyclotron and Alfvén waves over the polar regions, J. Geophys. Res., 106, p. 13,219.

Gurnett, D. A., W. S. Kurth, J. T. Steinberg, and S. D. Shawhan (1988), Plasma wave turbulence around the Shuttle: results from the Spacelab-1 flight, Geophys. Res. Lett., 15, p. 760.

Horwitz, J. L., C. W. Ho, H. D. Scarbro, G. R. Wilson, and T. E. Moore (1994), Centrifugal acceleration of the polar wind, J. Geophys. Res. 99(A8), 15051, 1994.

Hubert, D, and F. Leblanc (1997), The auroral O+ non-Maxwellian distribution function revisited, Ann. Geophys. 15, p. 249.

Isenberg, P. A., and B. J. Vasquez (2007), Preferential perpendicular ion heating of coronal hole minor ions by the Fermi mechanism, Ap. J. 668:pp.546-547.

Jeans, J. H. (1904), The Dynamical Theory of Gases, Cambridge Univ. Press.

Kelley, M. C., and R. A. Heelis (1989), The Earth's Ionosphere, Academic, San Diego, 1989.

Khazanov, G. V., M. W. Liemohn, and T. E. Moore (1997), Photoelectron effects on the self-consistent potential in the collisionless polar wind, J. Geophys. Res. , 102(A4), p. 7509,

Khazanov, G. V., M. W. Liemohn, E. N. Krivorutsky, and T. E. Moore, 1998, Generalized kinetic description of a plasma in an arbitrary field-aligned potential energy structure, J. Geophys. Res. 104(A4), p. 6871.

Kinzelin, E., and D. Hubert (1988), Instability of electrostatic and ion-cyclotron modes in the F region of the auroral ionosphere, Ann. Geophys. 6(3), 255.

Kivelson, M.G. and C.T. Russell 1995), Introduction to Space Physics, Cambridge Univ., 1995.

Lee, M. A., and S. P. Gary (1991), Quasi-linear evolution of ULF waves excited by cometary ion pick-up, J. Geophys. Res., v. 96(12), pp. 21319-21327.

Leer, E., and T. E. Holzer (1980), Energy Addition in the Solar Wind, J. Geophys. Res., 85, A9, p.4681.

Loranc, M, and J.-P. St.-Maurice (1993), A time-dependent gyro-kinetic model of thermal ion up-flows in the high-latitude F region, J. Geophys. Res., 99(A9), p.17,429.

Moore, T. E. (1980), Modulation of terrestrial ion escape flux composition, J. Geophys. Res., 85, A5, p. 2011, May 1, 1980.

Moore, T. E., J. H. Waite, Jr, M. Lockwood, and C. R. Chappell (1986), Observations of coherent transverse ion acceleration, Geophysical Monograph 38, Am. Geophys. Un., Washington, DC, p. 50.

Moore, T. E., M.O. Chandler, C.J. Pollock, D.L. Reasoner, R.L. Arnoldy, B. Austin, P.M. Kintner, and J. Bonnell, 1996, Plasma heating and flow in an auroral arc, J. Geophys. Res. 101(A3), p.579.

Moore, T. E., and J. L. Horwitz (2007), Stellar ablation of planetary atmospheres, Rev. Geophys., 45, RG3002, doi:10.1029/2005RG000194.

Mukai, T., et al. (1986), Plasma observation by Suesei of solar wind interaction with comet Halley, Nature, 321, p. 299.

Neugebauer, M. (1990), Spacecraft observations of the interaction of active comets with the solar wind, Revs. Geophys. 28, p.231.

Paterson, W. R., and L. A. Frank (1989), Hot ion plasmas from the cloud of neutral gases surrounding the space shuttle, 94(A4), p. 3721.

Post, R. F., and M. N. Rosenbluth (1966), Electrostatic instabilities in finite mirror confined plasmas, Phys. Fluids, 9, p.730.

Puhl, P, T. E. Cravens, and J. Lindgren (1993), Ion thermalization in the inner coma of a comet, Ap. J., 418, pp.899-911, Dec. 1.

Ridley, A. J.,T. I. Gombosi, and D. L. DeZeeuw (2004), Ionospheric control of the magnetosphere: conductance, Ann. Geophys. (2004) 22, pp. 567–584.

Richardson, I., et al. (1987), Observations of energetic water group ions at comet Giacobini-Zinner, Planet. Sp. Sci., 35, p.1323.

Shizgal, B.D., and Arkos, G.G. (1996), Nonthermal escape of the atmospheres of Venus, Earth, and Mars: Reviews of Geophysics, v. 34, no. 4, p. 483-505.

Strangeway R. J., et al. (2005), Factors controlling ionospheric outflows as observed at intermediate altitudes, J. Geophys. Res., A03221.

St.-Maurice, J.-P., and R. W. Schunk (1979), Ion velocity distributions in the high-latitude ionosphere, Rev. Geophys. Space Phys. 17, 99.

K. Suvanto, et al. (1989), Analysis of incoherent scatter radar data from non-thermal F-region plasma, Journal of Atmospheric and Terrestrial Physics, Vol. *51, No.* 6, pp. 483-495.

Szegö, K. et al. (2000), Physics of mass loaded plasmas, S*pace Science Reviews* 94**:** 429–671, 2000.

Wilson, G. R. (1994), Kinetic modeling of O^+ upflows resulting from ExB convection heating in the high-altitude F region ionosphere, J. Geophys. Res., 99, A9, pp. 17453.

Wilson, G. R., and P. Craven (1999), Molecular ion upflow in the cleft ion fountain, J. Geophys. Res., 104(A3), 4437–4446.

Winkler, E., J.-P. St-Maurice, and A. R. Barakat (1992), Results from improved Monte Carlo calculations of auroral ion velocity distributions, J. Geophys. Res., 97, p.8399.

Zeng, W, and J. L. Horwitz (2007), Formula representation of auroral ionospheric O+ outflows..., Geophys. Res. Lett. 34, L06103, doi:10.1029/2006GL028632.

Zheng Y., et al. (2005), Polar study of ionospheric ion outflow versus energy input, J. Geophys. Res., 110, A07210, doi:10.129/2004JA010995.

1 **Table 1. Assumed velocity distributions**

Distribution type	Definition (N = normalization)	Cumulative ($v_{esx} < v < \infty$)
Ring distribution in plasma frame ($v_\perp = v_{conv}$), N = normalization	$f(v_{//}, v_\perp) = N \exp\left(-(v_{//}^2 - (v_\perp - v_{conv})^2)/v_{th}^2\right)$	v_{esg} = gravitational v_{esc} = g less centrifugal v_{esa} = above less ambipolar
Lorentzian (generalized exponent, K)	$f(v_\perp) = N/\left(1 + (v_\perp / v_{conv})^{2K}\right)$	$1 - \frac{2}{\pi}\arctan(v_{esx}/v_{scl})^K$
Exponential	$f(v_\perp) = N \exp\left(-v_\perp / v_{conv}\right)$	$\exp(-V_{esx}/V_{scl})$
Thermalized	$f(v_\perp) = N \exp\left(-v_\perp^2 / v_{conv}^2\right)$	$erfc(V_{esx}/V_{th})$

2

Figures

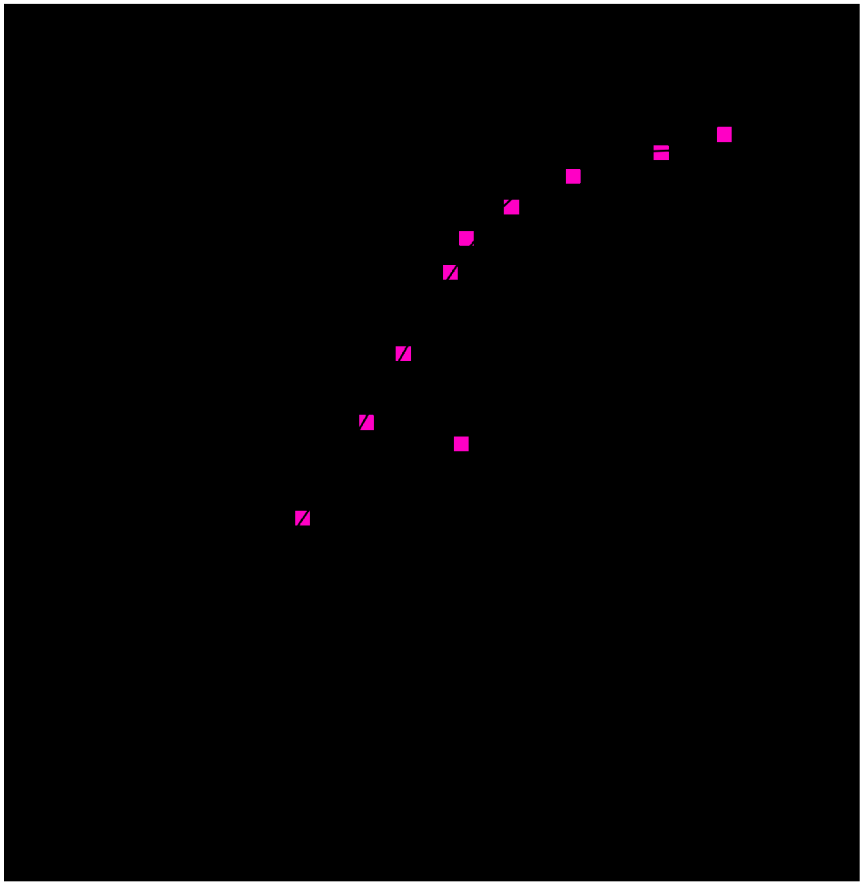

Figure 1. Ambipolar potential as a function of the fractional density of superthermal electrons after Khazanov et al. [1997], digitized from their figure 3.

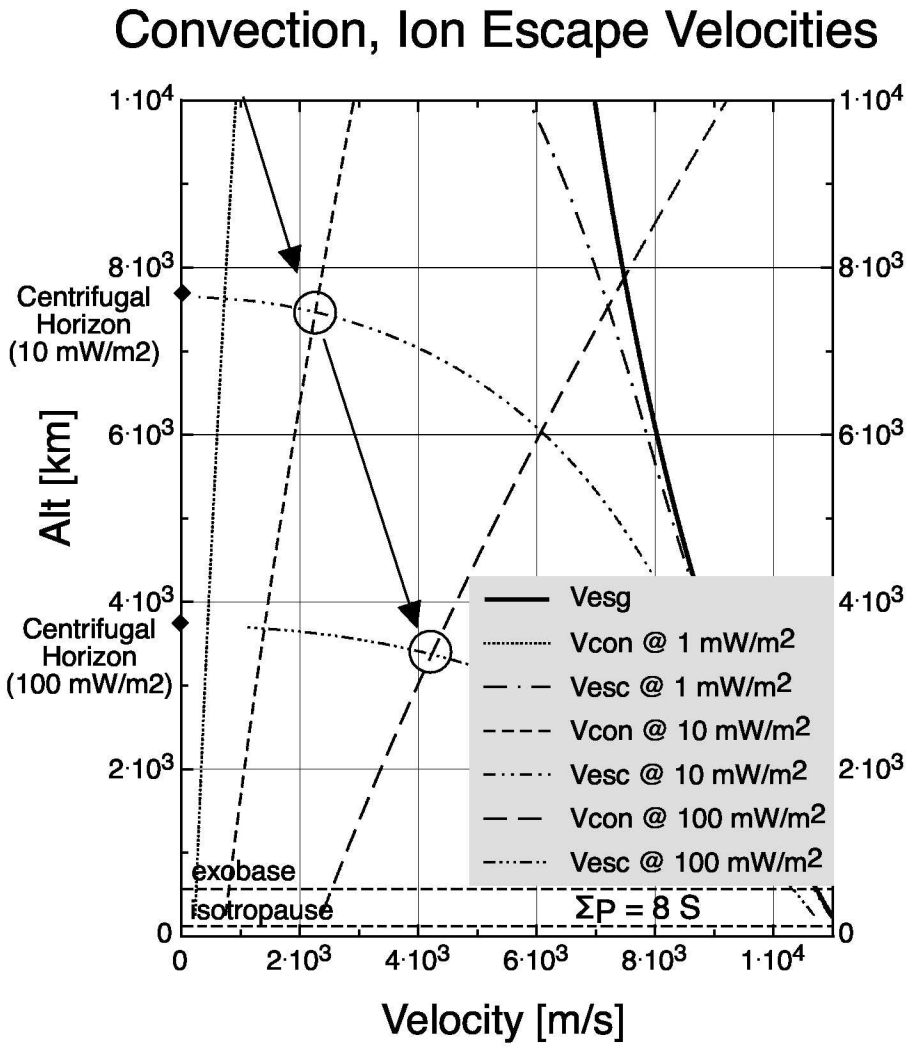

Figure 2. Altitude dependence of escape speed and convection speed for three values of Poynting Flux at 4000 km altitude, at a typical value of ionospheric height integrated conductivity (8 S). V_{esg} is the normal gravitational escape speed. V_{esc} is the escape speed when centrifugal acceleration is taken into account. Circles mark points where the ring beam speed exceeds the local escape speed.

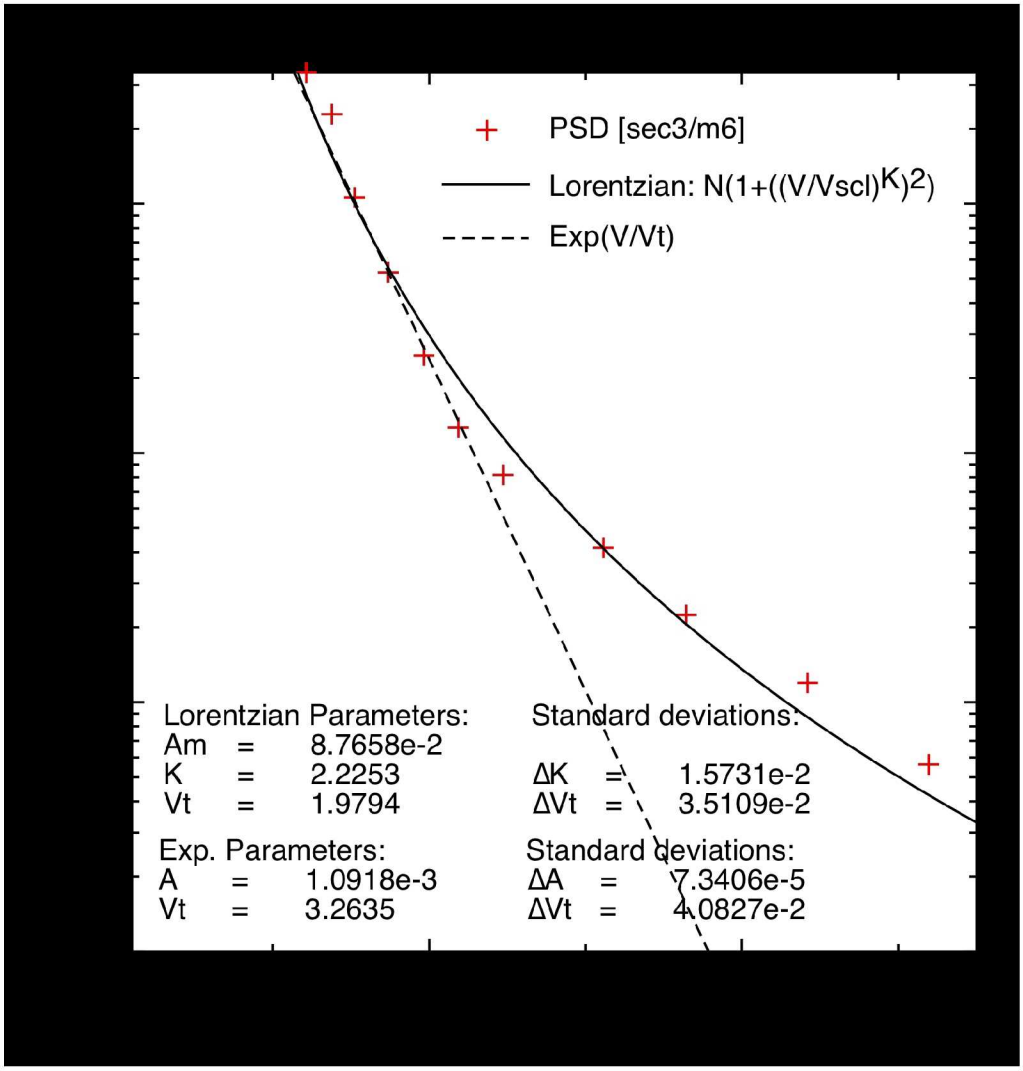

Figure 3. A representative example of the energy distribution of transversely accelerated ions [After André et al. 1994], from the Freja mission at about 1700 km altitude over the auroral zone. Exponential and Lorentzian fits are shown as smooth curves.

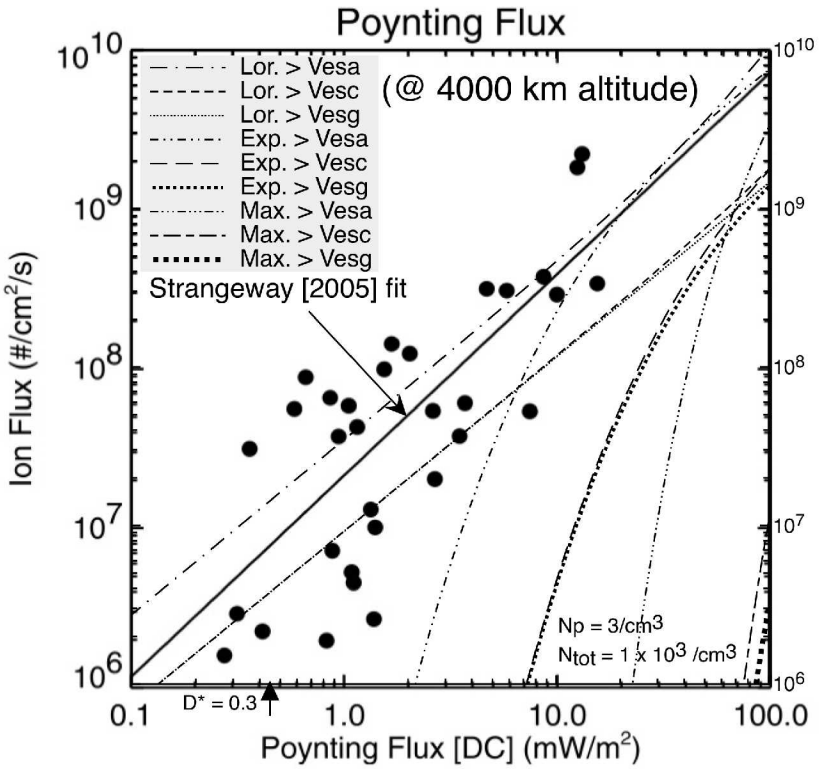

Figure 4. "Generalized Jeans escape" of O^+ escape flux vs. Poynting flux at 4000 km altitude, for three velocity distributions (Lorentzian, Exponential and Maxwellian ring beams), and for escape above three velocity thresholds: V_{esg}: gravitational only; V_{esc}: deducts centrifugal potential; V_{esa} deducts ambipolar potential. Data and fit from Strangeway et al., [2005] are included for comparison. Limiting flux is taken as 2×10^{10} cm^{-2} s^{-1}. Exobase is taken at 500 km altitude, and ambipolar potential above 500 km is 6.5 V corresponding to a precipitating electron density of $3/cm^3$ and $N_p/N_{tot} = 0.3\%$. Poynting flux corresponding to D* = 0.3 is indicated for reference.

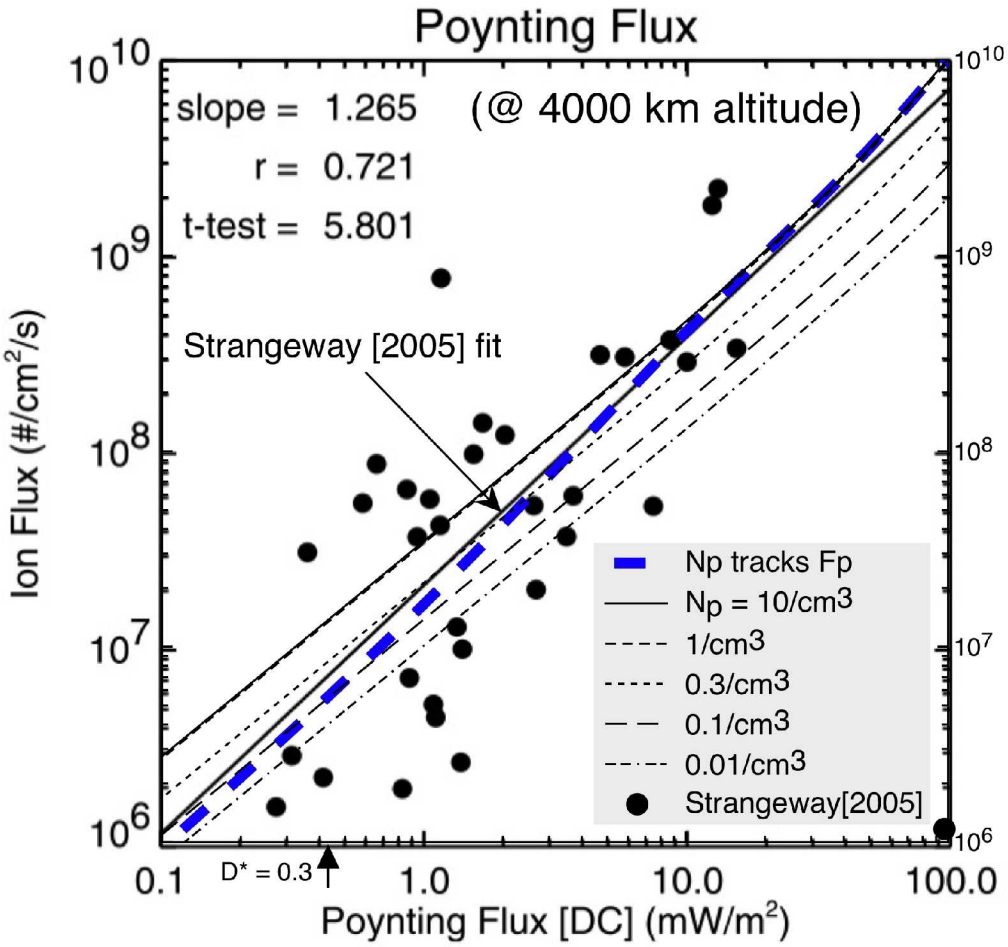

Figure 5. Similar to Figure 4, but with multiple traces reflecting Lorentzian velocity distributions, with the indicated values of precipitating electron density, Np. The trace for Np = 1 cm^{-3} is the same as the Lorentzian trace on Figure 4. The bold dashed curve if for Np tracking PF per Strangeway et al. [2005], that is, for Np = $(2.14\ 10^7 \times PF^{1.265}/1.02 \times 10^9)^{(1/2.2)}$

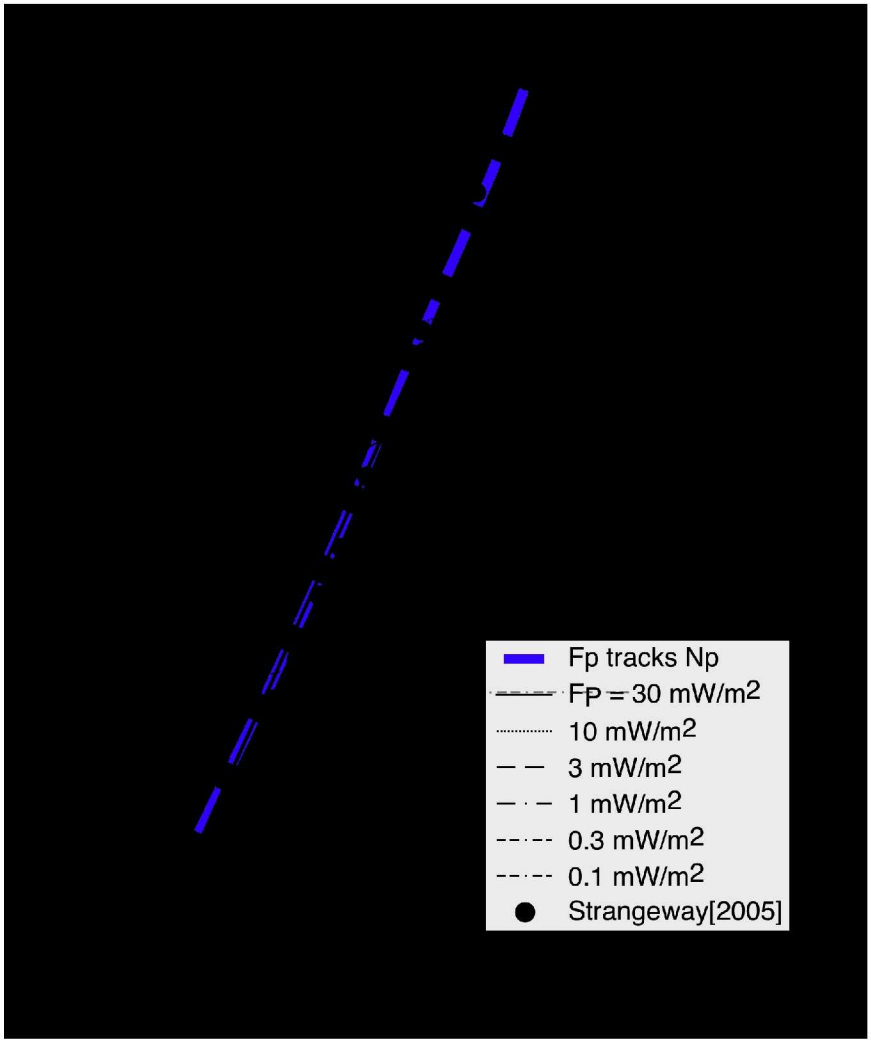

Figure 6. "Generalized Jeans escape" estimate of O^+ escape flux dependence upon precipitating electron density at 4000 km altitude, for multiple traces based on the indicated values of Poynting flux, assuming Lorentzian velocity distributions. Data and fit from Strangeway et al., [2005] are included for comparison. The limiting flux is taken as 2×10^{10} cm^{-2} s^{-1}. The exobase is taken at 500 km altitude.

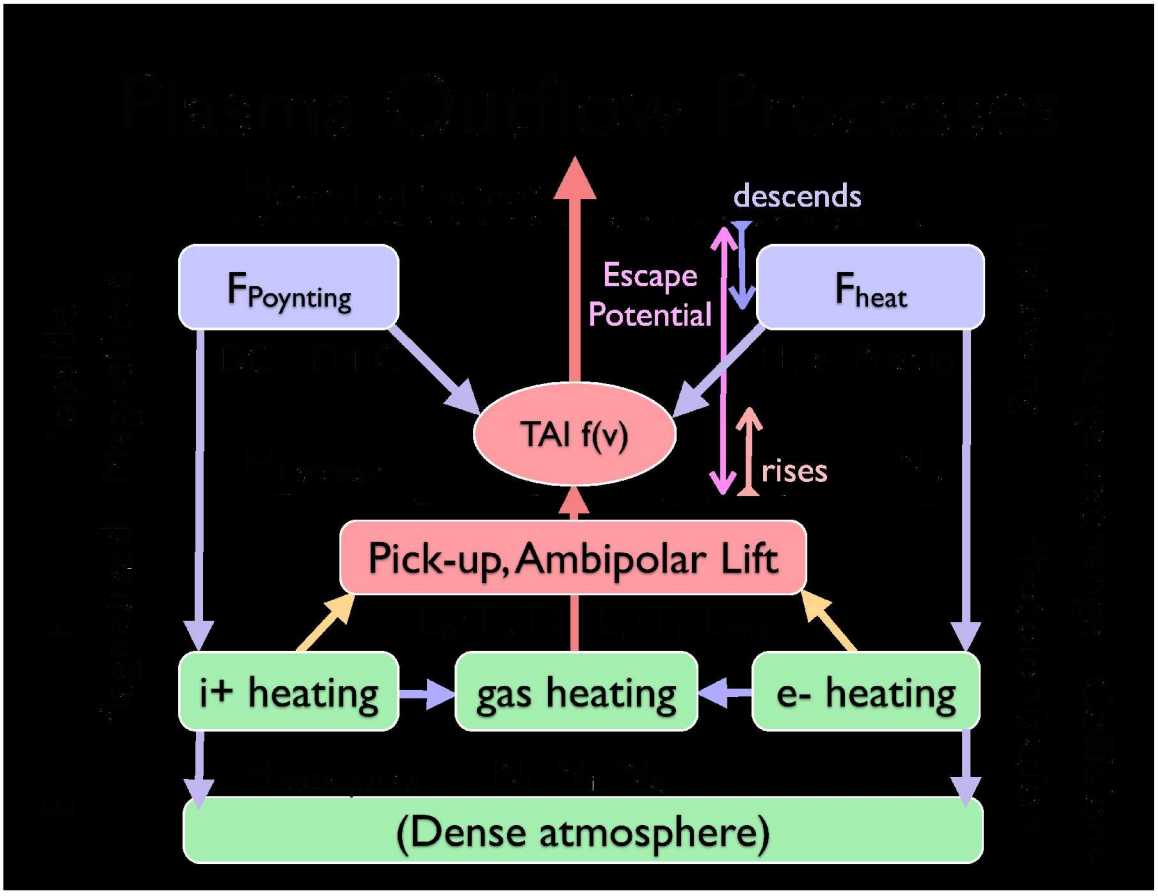

Figure 7. Schematic diagram of ionospheric outflow mechanisms illustrating the role of ion pick-up, ambipolar electric field, and centrifugal forcing in the outflow of ionospheric plasma. The flow chart is derived from that given by Strangeway et al. [2005].

Figure Captions

Figure 1. Ambipolar potential as a function of the fractional density of superthermal electrons after Khazanov et al. [1997], digitized from their figure 3.

Figure 2. Altitude dependence of escape speed and convection speed for three values of Poynting Flux at 4000 km altitude, at a typical value of ionospheric height integrated conductivity (8 S). V_{escg} is the normal gravitational escape speed. V_{escc} is the escape speed when centrifugal acceleration is taken into account. Circles mark points where the ring beam speed exceeds the local escape speed.

Figure 3. A representative example of the energy distribution of transversely accelerated ions [After André et al. 1994], from the Freja mission, observed at about 1700 km altitude over the auroral zone. Exponential and Lorentzian fits are shown.

Figure 4. "Generalized Jeans escape" of O^+ escape flux vs. Poynting flux at 4000 km altitude, for three velocity distributions (Lorentzian, Exponential and Maxwellian ring beams), and for escape above three velocity thresholds: V_{esg}: gravitational only; V_{esc}: deducts centrifugal potential; V_{esa} deducts ambipolar potential. Data and fit from Strangeway et al., [2005] are included for comparison. Limiting flux is taken as 2×10^{10} cm^{-2} s^{-1}. Exobase is taken at 500 km altitude, and ambipolar potential above

500 km is 6.5 V corresponding to a precipitating electron density of $3/cm^3$ and N_p/N_{tot} = 0.3%. Poynting flux corresponding to D* = 0.3 is indicated for reference.

Figure 5. Similar to Figure 4, but with multiple traces reflecting Lorentzian velocity distributions, with the indicated values of precipitating electron density, Np. The trace for Np = 1 cm^{-3} is the same as the Lorentzian trace on Figure 4. The bold dashed curve if for Np tracking PF per Strangeway et al. [2005], that is, for Np = $(2.14\ 10^7 \times PF^{1.265}/1.02 \times 10^9)^{(1/2.2)}$

Figure 6. "Generalized Jeans escape" estimate of O^+ escape flux dependence upon precipitating electron density at 4000 km altitude, for multiple traces based on the indicated values of Poynting flux, assuming Lorentzian velocity distributions. Data and fit from Strangeway et al., [2005] are included for comparison. The limiting flux is taken as 2×10^{10} cm^{-2} s^{-1}. The exobase is taken at 500 km altitude.

Figure 7. Schematic diagram of ionospheric outflow mechanisms illustrating the role of ion pick-up, ambipolar electric field, and centrifugal forcing in the outflow of ionospheric plasma. The flow chart is derived from that given by Strangeway et al. [2005].